EC
Journals.ASM.org

Bestatin Inhibits Cell Growth, Cell Division, and Spore Cell Differentiation in *Dictyostelium discoideum*

Yekaterina Poloz,[a] Andrew Catalano,[a] and Danton H. O'Day[a,b]

Department of Cell and Systems Biology, University of Toronto, Toronto, Ontario, Canada,[a] and Department of Biology, University of Toronto Mississauga, Mississauga, Ontario, Canada[b]

Bestatin methyl ester (BME) is an inhibitor of Zn^{2+}-binding aminopeptidases that inhibits cell proliferation and induces apoptosis in normal and cancer cells. We have used *Dictyostelium* as a model organism to study the effects of BME. Only two Zn^{2+}-binding aminopeptidases have been identified in *Dictyostelium* to date, puromycin-sensitive aminopeptidase A and B (PsaA and PsaB). PSA from other organisms is known to regulate cell division and differentiation. Here we show that PsaA is differentially expressed throughout growth and development of *Dictyostelium*, and its expression is regulated by developmental morphogens. We present evidence that BME specifically interacts with PsaA and inhibits its aminopeptidase activity. Treatment of cells with BME inhibited the rate of cell growth and the frequency of cell division in growing cells and inhibited spore cell differentiation during late development. Overexpression of PsaA-GFP (where GFP is green fluorescent protein) also inhibited spore cell differentiation but did not affect growth. Using chimeras, we have identified that nuclear versus cytoplasmic localization of PsaA affects the choice between stalk or spore cell differentiation pathway. Cells that overexpressed PsaA-GFP (primarily nuclear) differentiated into stalk cells, while cells that overexpressed PsaAΔNLS2-GFP (cytoplasmic) differentiated into spores. In conclusion, we have identified that BME inhibits cell growth, division, and differentiation in *Dictyostelium* likely through inhibition of PsaA.

The social amoebozoan *Dictyostelium discoideum* has long been a model organism for the study of fundamental cellular processes, including cell division, motility, differentiation, and morphogenesis (22, 23). More recently, it has been shown to be a useful organism for the elucidation of disease processes, including Huntington's and Alzheimer's diseases (29, 31, 53). It has also provided new insight into the mode of action of various drugs such as valproic acid and lithium, which are widely used mood stabilizers (50, 53). The use of pharmaceuticals is especially valuable in this microorganism when gene knockouts are ineffective (18). Recently, *D. discoideum* puromycin-sensitive aminopeptidase (Psa) was partially characterized; however, the effects of bestatin which targets this enzyme have not been studied (7).

Bestatin is a specific inhibitor of Zn^{2+}-binding aminopeptidases (5, 49, 52). Bestatin methyl ester (BME) is a more cell permeable analog of bestatin (45). Treatment of several different cell types with bestatin or BME inhibits cell proliferation and induces apoptosis (10, 25, 30, 45, 55). Bestatin has previously been shown to inhibit PSA function in COS cells (10). Currently, bestatin is used in the treatment of acute myeloid leukemia and lung squamous cell carcinoma (2, 15, 20, 45). It may also find future uses in the treatment of lung adenocarcinoma, esophageal adenocarcinoma, choriocarcinoma, and uterine cervical carcinoma (9, 11, 21, 51). Bestatin also has anti-inflammatory properties, as it modulates the production of cytokines and chemokines by monocytes and macrophages (26).

PSA is an exopeptidase that belongs to the M1 family of Zn^{2+}-binding aminopeptidases (10, 42). It cleaves amino acids from the N terminus of oligopeptide chains. In COS cells and Swiss 3T3 fibroblasts it localizes to the nucleus and the cytoplasm (10). PSA is involved in proteolytic events that mediate processes like cell cycle progression in mitosis and meiosis, embryogenesis, neuronal differentiation, establishment of polarity, reproduction, and processing of major histocompatibility complex class I peptides in a variety of organisms (4, 10, 19, 27, 38, 39, 43, 44). In addition, it may have roles in cell signaling and protein trafficking, independent of its enzymatic activity (40). Additionally, PSA has been identified as the primary aminopeptidase responsible for the digestion of poly(Q) repeats released by proteasomes in neurons and thus is implicated in poly(Q) diseases like Huntington's (3). It has also been shown to digest neuronal tau and is implicated in Alzheimer's disease and other tauopathies (24).

Two homologs of mammalian PSA have been identified in *D. discoideum* and termed PsaA and PsaB (7). An alignment of *D. discoideum* PsaA with PSA from other species has revealed the presence of a conserved exopeptidase GAMEN motif, a Zn^{2+}-binding domain, one putative nuclear export signal (NES), and at least one nuclear localization signal (NLS2) (7). We previously reported the generation of an anti-PsaA antibody and PsaA-GFP (where GFP is green fluorescent protein) fusion protein-expressing strains (7). With the help of both we have identified that PsaA is distributed mainly throughout the nucleoplasm and to a lesser extent the cytoplasm in growing cells and redistributes throughout the cytoplasm during mitosis. PsaA is also distributed mainly throughout the nucleoplasm and to a lesser extent the cytoplasm in prestalk and prespore cells in slugs and stalk and spore cells in fruiting bodies. We generated a strain expressing PsaAΔNLS2-GFP, a deletion mutant of PsaA that lacks NLS2. The removal of NLS2 resulted in the inability of PsaA to enter the nucleus and its subsequent accumulation in the cytoplasm in growing and devel-

Received 7 December 2011 **Accepted** 11 February 2012
Published ahead of print 17 February 2012
Address correspondence to Danton H. O'Day, danton.oday@utoronto.ca.

doi:10.1128/EC.05311-11

oping cells (7). As in other cells, PsaA may regulate cell cycle progression and cell differentiation in *D. discoideum*. Further evidence for the potential role of PsaA in cell cycle regulation and cell differentiation comes from a recent finding that PsaA interacts and colocalizes with nucleomorphin (NumA1) and cyclin-dependent kinase 5 (Cdk5) (7, 17). NumA1 is an acidic, nucleolar Ca^{2+}-dependent calmodulin-binding protein (CaMBP) (33). Several pieces of evidence suggest that it regulates cell cycle in *D. discoideum* (6, 32, 33). NumA1 is also expressed throughout development, its expression is regulated by DIF-1, and it interacts with a prestalk O (pstO)-specific protein Ca^{2+}-binding protein 4a (CBP4a) (32, 34, 37). Thus, NumA1 likely regulates the cell cycle and plays a role in pstO cell differentiation. Cdk5 is a nucleoplasmic and cytoplasmic protein that regulates growth and spore cell differentiation in *D. discoideum* (17, 18, 46).

Our goal is to identify the effect of bestatin on *D. discoideum* cell division and differentiation, as well as to gain further insight into the role of PsaA in these processes.

MATERIALS AND METHODS

Chemicals, strains, and culture conditions. All generic chemicals were obtained from BioShop Canada (Burlington, ON, Canada) or Sigma-Aldrich (St. Louis, MO). BME was purchased from Santa Cruz Biotechnologies (Santa Cruz, CA). *D. discoideum* PsaA-GFP, PsaAΔNLS2-GFP, GFP, and the parental AX3 strains were all maintained on Sussman's medium (SM) agar plates in association with *Escherichia coli* B/r at 21°C in the dark. For the selection of GFP strains, 100 μg/ml G418 was added to the SM plates. Alternatively, all strains were maintained axenically in HL-5 medium, shaking at 180 rpm at 21°C. For the selection of GFP strains, 10 μg/ml G418 was added to the HL-5 medium. The expression of all GFP constructs is governed by the constitutively active actin-15 promoter.

Measurements of cell density, cell growth, and doubling time. Growing cells (1×10^6 to 2×10^6 cells/ml) were diluted to 1.0×10^3 cells/ml and transferred (3 ml) into a well in a 12-well multiwell plate (2.5-cm diameter/well). Cells were treated with 0, 10, 50, 100, 300, or 600 μM BME and allowed to grow at 21°C shaking at 180 rpm for 48 h. A hemocytometer was used to measure cell density after 0, 24, and 48 h. For nuclear counting, cells were fixed in ultracold methanol and mounted using ProLong Gold antifade with DAPI (4′,6-diamidino-2-phenylindole) (Invitrogen). Cells were observed using the Nikon Eclipse 50i microscope with the mounted Nikon Digital Sight DS-Ri1 camera, and nuclei were counted and measured using the NIS Elements 3.2Br software (Nikon, Melville, NY).

Immunolocalizations. The immunolocalization of PsaA, NumA1, and tubulin was performed according to a previously described protocol (7). Cells were fixed, blocked, and incubated with anti-PsaA or anti-NumA1 (1:20 or 1:40, respectively), followed by either Alexa Fluor 555 or 488 secondary antibodies (1:40; Invitrogen, Burlington, ON, Canada). Cells were then incubated with anti-α-tubulin (1:100; Developmental Studies Hybridoma Bank), followed by Alexa Fluor 555 or 488 secondary antibody (1:100; Invitrogen). Coverslips with cells were mounted using ProLong Gold antifade (Invitrogen) containing DAPI. Slides were viewed, and cell images were captured using the Nikon Eclipse 50i microscope with the mounted Nikon Digital Sight DS-Ri1 camera.

Viability staining. Cells were harvested after treatment with the different concentrations of BME for 24 h and were stained with 20 μg/ml fluorescein diacetate and propidium iodide for 5 min. Cells were deposited onto slides and viewed using the Nikon Eclipse 50i microscope with the mounted Nikon Digital Sight DS-Ri1 camera. At least 100 cells were counted for each treatment.

Fluorometric aminopeptidase assay. Cells were harvested, washed, and lysed in NP-40 lysis buffer (50 mM Tris-HCl [pH 7.5], 150 mM NaCl, 0.5% NP-40). Total cell protein was quantified using the Bradford assay and 1-mg/ml protein aliquots were made. Ten microliters of total cell protein was mixed with 290 μl of substrate solution (0.1 mg/ml dithiothreitol [DTT], 0.1 mg/ml albumin, and 1 mM alanine-β-naphthylamide) (1). Fluorometric measurements (340 nm excitation, 400 nm emission) were made after 15 and 30 min. The slope of the line between the 15- and 30-min measurements was used to represent aminopeptidase activity. Total cell protein was preincubated with bestatin, amastatin, puromycin, EDTA, and/or $ZnCl_2$ for 20 min before the fluorometric aminopeptidase assay.

Synchronized development of cells. Cells were harvested, washed, and plated at 2×10^7 cell/ml onto black membrane filters (Millipore, Billerica, MA) as detailed elsewhere (12). Filter pads were soaked in $ddH_2O \pm$ BME. Development was allowed to proceed for 24 h. For the generation of chimeras, cells of different strains were harvested separately and mixed in a range of ratios with the parental AX3 (1:9 to 9:1) before plating. Generation of chimeras is a widely used and very powerful tool in the analysis of regulation of cell differentiation in *Dictyostelium* (14). Membrane filters were propped at a 90-degree angle for side-view photography. The structures formed by 24 h were stained with 0.01% calcofluor (Ciba-Geigy, now Novartis, Basel, Switzerland) before being viewed and photographed. A Nikon Eclipse 50i microscope with the mounted Nikon Digital Sight DS-Ri1 camera (Nikon, Melville, NY) was used to view and capture all images. Slug fluorescence scans were done using the profile tool of NIS Elements 3.2Br software. All slug lengths were standardized to 1 in Excel (Microsoft Office), and average fluorescence intensity values were calculated for each 0.1 of the slug's length. Spore shapes were measured using the measurements tool of NIS Elements 3.2Br software.

Northern blotting. Total RNA was isolated from growing and developing cells, separated in a 1% agarose-formaldehyde gel (25 μg/lane), transferred onto a positively charged nylon membrane, and fixed onto the membrane via UV-cross-linking according to a previously described method (41). Northern blotting was performed according to a previously described method with a few modifications (41). The following primers were used for PCR amplification of DNA probes: *psaA* F, GGTGAATCATTTAGAAAGGGTC; R, CTAAACGATCTTGAGCT GGAAG; *rnlA* F, AGGGTTACGCGATCGCTAA; R, TTCGCTACCT TAGGACCGTC. Digoxigenin (DIG)-labeling and purification were followed by the prehybridization (2 h) and hybridization (overnight) at 42°C. The blots were exposed to Bioflex MSI film for 5 min (Clonex Corporation, Markham, ON, Canada) and developed using CB^2 developer and Chemblend fixer (Simon, Baltimore, MA). Blots were scanned and band intensities were quantified using ImageQuant Pro 5.2 (GE Healthcare, Baie d'Urfe, QC, Canada).

Western blotting. For the analysis of developmental levels of PsaA, 2×10^6 growing and developing cells were harvested and lysed with NP-40 lysis buffer. For the analysis of effect of morphogens on PsaA expression, growing cells were washed and resuspended in KK_2 at a concentration of 2×10^6 cells/ml. Cell numbers were counted in a hemocytometer. The compounds used in the different experiments were added in the same buffer at the indicated concentrations (20 mM NH_4Cl, 1 mM cyclic AMP [cAMP], or 100 nM DIF-1). Cells were starved in KK_2 at 22°C with shaking at 250 rpm to reduce cell-cell contact and harvested at 2 and 4 h posttreatment. Cells were also lysed with NP-40 lysis buffer. The rest of the procedure was conducted as previously described (37). Samples were separated on 12% SDS-PAGE gel (25 μg/lane), transferred onto polyvinylidene difluoride (PVDF) membrane, and probed with rabbit anti-PsaA (1:500) (7), mouse anti-α-tubulin (1:1,000, 12G10; Developmental Studies Hybridoma Bank, Iowa City, IA), or mouse anti-GFP (1:600; Santa Cruz Biotechnologies). Membranes were developed with the Amersham ECL Plus western blotting detection system (GE Healthcare, Buckinghamshire, United Kingdom) and scanned using a Storm 860 phosphorimager/fluorimager (Molecular Dynamics Inc., Sunnyvale, CA). Blots were analyzed, and the band intensities were quantified using ImageQuant Pro 5.2.

Statistical analysis. All statistical analyses were performed using Student's *t* test or one-way analysis of variance (ANOVA) followed by Tukey's test in Minitab15 or 16 (Minitab, State College, PA).

RESULTS

BME-treated cells progress slower through the cell cycle due to decreased rate of cell growth and the frequency of cell division. In order to examine the effects of BME on growth, cells were treated with a range of concentrations and cell density was measured. In untreated cultures, cell density increased 18.46-fold in 48 h; however, increasing BME concentration resulted in a smaller increase in cell density, with 600 μM resulting in only a 3.25-fold increase after 48 h (Fig. 1A). This represents an 82.3% inhibition by BME. To clarify whether BME treatment decreases the frequency of cell division, resulting in increased doubling time, the doubling time of BME-treated cells in log phase was calculated from the data obtained between 24 and 48 h in Fig. 1A. Doubling time increased with increasing BME concentration to a maximum of 3.70-fold, from 8.22 $\pm$ 0.96 h at 0 μM to 30.41 $\pm$ 3.07 h at 600 μM (Fig. 1B).

A decreased frequency of cell division would result in a longer interphase, and if the growth rate was unaffected, cells would thus be larger. However, BME-treated cells were the same size as untreated cells, meaning their growth rate must also have been slower than untreated cells (Fig. 1C). Fittingly, BME-treated cells (600 μM) possessed nucleoli 0.23-fold smaller (4.69% $\pm$ 0.93% of nuclear area) than untreated cells (20.07% $\pm$ 2.93%), a phenomenon associated with slow growth in human cells (Fig. 2A to C) (28). Together, these results show that BME treatment results in a slower progression through the cell cycle resulting from both a lower rate of growth and a decreased frequency of cell division.

Multinuclearity in *D. discoideum* obscures the effect of BME. Upon examining the effects of BME on cell morphology it appeared as though BME-treated cells were smaller; however, the difference was due to the decreased number of multinucleate cells. Multinuclearity in *D. discoideum* axenic liquid cultures is generally thought to be a result of impaired cytokinesis due to the lack of substratum. Fittingly, the cell area in multinucleate cells was found to be proportional to the number of nuclei (Fig. 3A). The proportion of mononucleated cells in a BME-treated culture increased with increasing concentration to a maximum of 2.23-fold (from 38.89% $\pm$ 4.81% at 0 μM to 86.67% $\pm$ 6.54% at 600 μM) (Fig. 3B). This difference in the proportion of multinucleate cells thus masks the true effect of BME on cell growth. Ignoring aberrant cytokinesis and measuring the concentration of nuclei in a culture instead of the concentration of cells shows that, after 48 h, the concentration of nuclei in a BME-treated (600 μM) culture is 0.11-fold (89% inhibition) that of the untreated culture, as opposed to 0.18-fold (82% inhibition), as would be calculated by measuring cell concentration (Fig. 3C). Thus, BME inhibits the frequency of mitosis and the inherent multinuclearity in *D. discoideum* axenic cultures obscured the effect of BME.

BME is not cytotoxic to *D. discoideum* cells. In order to determine if BME was cytotoxic, BME-treated cells were double stained with fluorescein diacetate (FDA) and propidium iodide (PI). FDA is cleaved in live cells and fluoresces green. PI is a fluorescent nuclear stain that can only enter cells with compromised cell membrane permeability, and thus dying or dead. No dying cells were detected in untreated cultures or cultures treated with 10, 50, or 100 μM BME (Fig. 4A). Cultures treated with either 300 μM or 600 μM BME contained 99.14% $\pm$ 1.22% or 95.78% $\pm$ 3.25% live cells, respectively (Fig. 4A). As well, cells were observed in all stages of the cell cycle in cultures treated with 0, 10, 50, 100, 300, or 600 μM BME (Fig. 4B). Thus, BME is not cytotoxic to cells and its inhibition of cell culture growth was due to decreased frequency of mitosis, resulting in an increased cell doubling time, as opposed to cell death.

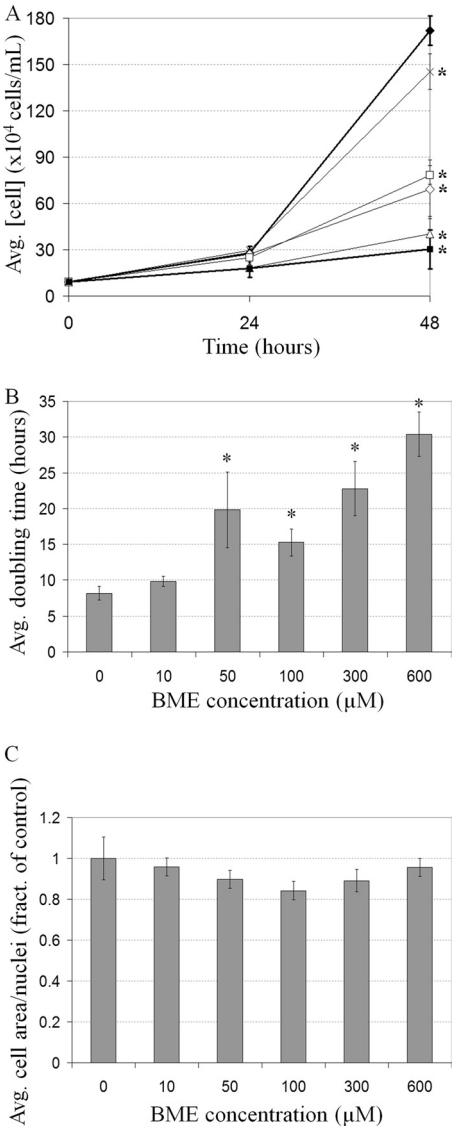

FIG 1 The effect of BME on *D. discoideum* growth. (A) The effect of BME on the increase in cell density over 48 h in untreated cells (black diamonds) or cells treated with either 10 (cross), 50 (white diamonds), 100 (white squares), 300 (white triangles), or 600 μM (black squares) BME (mean + standard deviations [SD]). Student's *t* test was used to identify 48-h cell density values significantly different from the control (untreated cells) (*, *P* value $\leq$ 0.05). This experiment was independently replicated 3 times. (B) The effect of BME on the average cell doubling time (mean + SD). Student's *t* test was used to identify the doubling times significantly different from the control (untreated cells) (*, *P* value $\leq$ 0.05). (C) The effect of BME on cell size. The values represent the average cell area divided by the nuclear number (mean + SD). None of the values were found to be significantly different from the control (untreated cells) through Student's *t* test. At least 100 cells were viewed from 3 independent replicates.

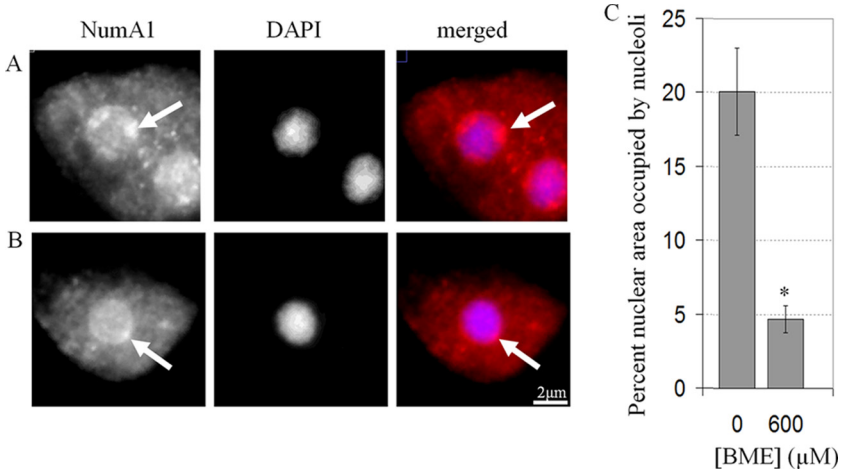

FIG 2 The effect of BME on nucleolar size in *D. discoideum*. NumA1, a nucleolar protein, was immunolocalized (red) in untreated cells (A) or cells treated with 600 μM BME (B). Cells were counterstained with DAPI (blue). (C) A quantification of the percentage of nuclear area of each cell that was occupied by nucleoli in untreated cells and cells treated with 600 μM BME (mean + SD). Student's *t* test was used to identify the significant difference in the percentage of nuclear area occupied by nucleoli in BME-treated cells (*, *P* value $\leq$ 0.05). At least 100 cells were viewed from 3 independent replicates.

BME affects spore cell differentiation. AX3 cells were allowed to develop on filters soaked in 600 or 900 μM BME. Agents are often used at up to 10 times the concentration for developmental studies in *D. discoideum* to account for the diffusion differences from the developmental substratums. Cells developed normally and formed fruiting bodies by 24 h in untreated and treated cultures (Fig. 5A). The fruiting bodies were stained with calcofluor to analyze the morphology of formed stalk and spore cells. Calcofluor is a fluorescent cellulose-specific stain that allows the visualization of cellulose walls of stalk and spore cells that form during terminal differentiation (16). Spores were rounder in 600 μM BME-treated cells than in the untreated controls (Fig. 5B and C). Nine hundred micromolar BME inhibited terminal spore cell differentiation, as no terminally differentiated spores were found in the spore mass (Fig. 5B). Thus, BME inhibits spore cell differentiation in *D. discoideum*.

Evidence that BME interacts with PsaA. PsaA was not detected by anti-PsaA in the nucleoplasm of BME-treated (600 μM) cells, suggesting that either PsaA is absent from the nucleoplasm in these cells or that BME-binding blocks anti-PsaA from detecting PsaA (Fig. 6A and B). The presence of PsaA-GFP in the nucleoplasm of BME-treated (600 μM) cells suggests that the latter is true and strongly implies an interaction between BME and PsaA (Fig. 6C and D).

PsaA is a puromycin-sensitive aminopeptidase, and BME inhibits its activity. A fluorometric assay with alanine-β-naphthylamide as a substrate was used to analyze aminopeptidase activity in whole-cell lysates of PsaA-GFP, GFP, and AX3 cells. Generation of actin 15 promoter-driven PsaA-GFP- and GFP-expressing strains has been previously described (7). Here aminopeptidase activity in these strains was detected, as measured by the liberation of naphthylamide after cleavage of alanine. Lysates of cells overexpressing PsaA-GFP had over 2-fold (229.97% $\pm$ 41.3%) more aminopeptidase activity compared to lysates of parental AX3 cells (Fig. 7A). Lysates of cells overexpressing GFP alone had the same level (95.33% $\pm$ 6.2%) of aminopeptidase activity as AX3 cell

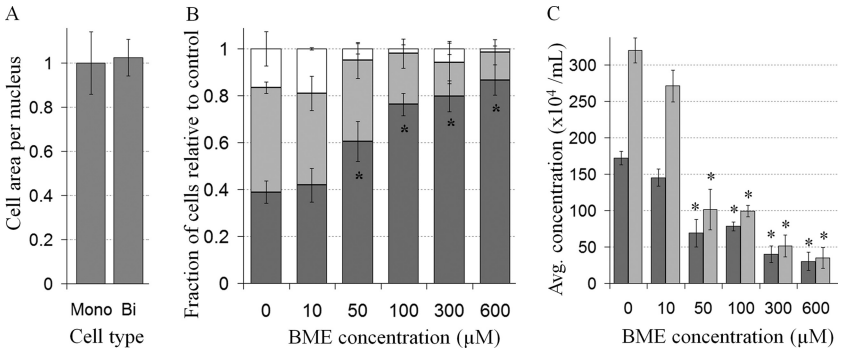

FIG 3 Multinuclearity in *D. discoideum* obscures the effect of BME on cell growth. (A) Cell area per nucleus in untreated cells was calculated by dividing cell area by the nuclear number in mononucleated (Mono) and binucleate (Bi) cells (mean + SD). (B) The proportion of mononucleated cells (dark gray), binucleate cells (light gray), or cells with more than two nuclei (white) in untreated cultures (0) or cultures treated with different concentrations of BME (mean + SD). Student's *t* test was used to identify a significant difference in the number of mononucleated cells in BME-treated cultures relative to control (untreated cultures) (*, *P* value $\leq$ 0.05). (C) Cell concentration (dark gray) and nuclear concentration (light gray) in cultures of untreated cells (0) or cells treated with different concentrations of BME (mean + SD). Student's *t* test was used to identify a significant difference in the concentrations of cells and nuclei in BME-treated cultures relative to control (untreated cultures) (*, *P* value $\leq$ 0.05). At least 100 cells were viewed from 3 independent replicates.

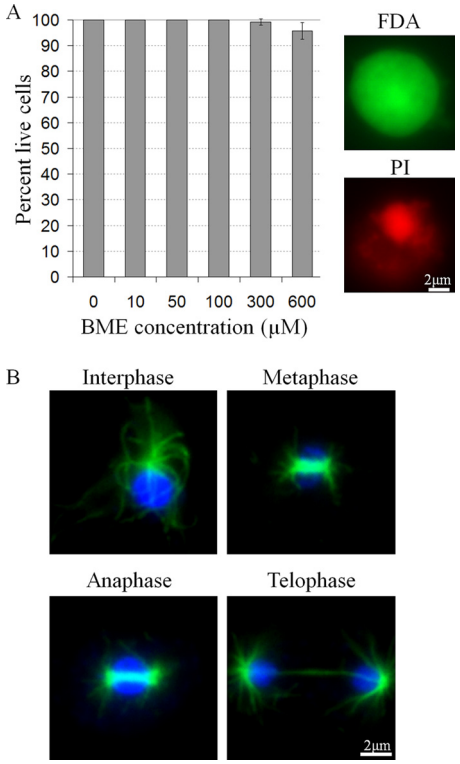

FIG 4 The effect of BME on cell viability in *D. discoideum*. (A) Percent live cells in BME-treated cultures after 24 h (mean + SD). All cells were double stained with FDA and PI. Representative cells showing FDA and PI staining, respectively, are shown on the right. At least 100 cells were viewed and counted from 3 independent replicates. (B) The presence of cells in all mitotic stages in BME-treated cultures. Tubulin (green) was immunolocalized, and the cells were counterstained with DAPI (blue). Representative cells from 600 μM BME-treated cultures are shown.

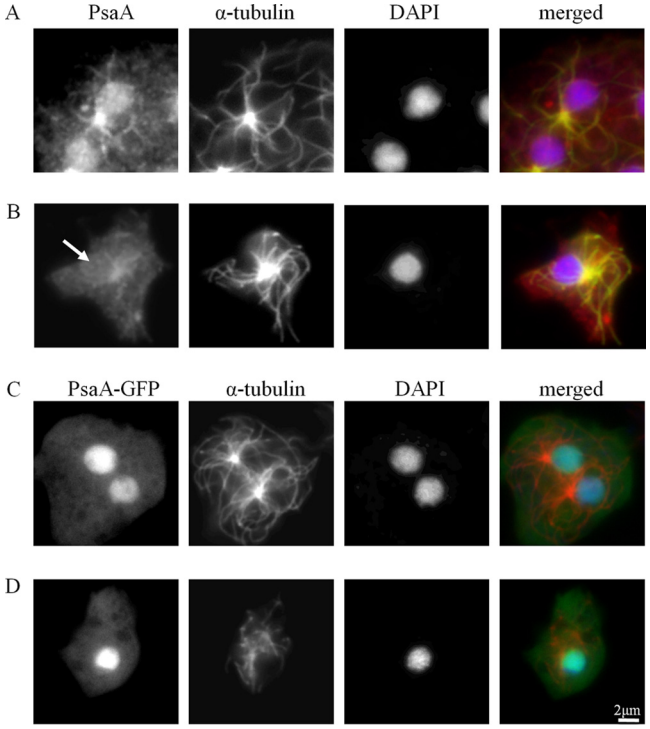

FIG 6 The effect of BME on the detection of PsaA via immunofluorescence. Untreated AX3 cells (A) or cells treated with 600 μm BME (B) were fixed and probed with anti-PsaA (red) and anti-α-tubulin (green) and counterstained with DAPI (blue). Nuclear PsaA was not detected in cells treated with BME (arrow). Nuclear localization of PsaA-GFP in untreated cells (C) and 600 μm BME-treated cells (D). The same procedure as in panels A and B was used. Anti-PsaA (green), anti-α-tubulin (red), and DAPI (blue). At least 100 cells were viewed from 3 independent replicates.

lysates. This suggests that PsaA is an alanine aminopeptidase that is overexpressed in the PsaA-GFP strain. Puromycin inhibited aminopeptidase activity in lysates of PsaA-GFP cells by 39.39% ± 3.1% of untreated control enzyme (Fig. 7B). In lysates of GFP-overexpressing cells, puromycin inhibited activity by 17.68% ± 1.9% of control. Thus, lysates of PsaA-GFP-overexpressing cells are more sensitive to the inhibition of aminopeptidase activity by puromycin than lysates of GFP-overexpressing cells.

The same difference in the sensitivity to inhibition was seen

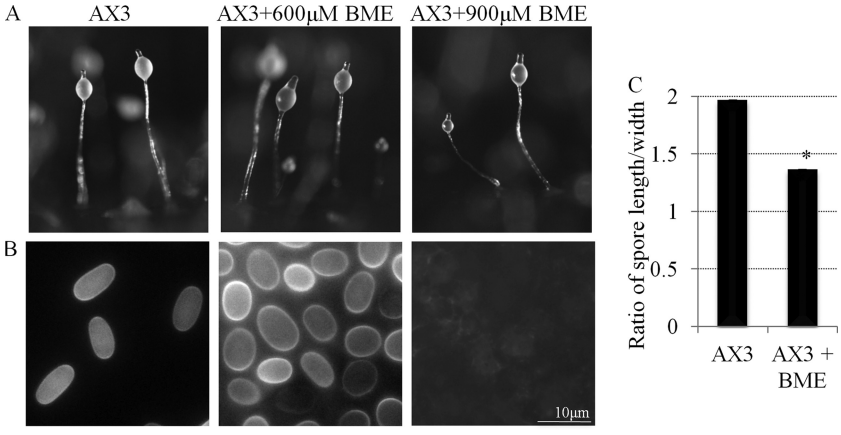

FIG 5 The effect of BME on *D. discoideum* development and spore cell differentiation. (A) Fruiting bodies formed by 24 h by untreated AX3 cells and AX3 cells treated with 600 or 900 μM BME. (B) Calcofluor-stained spores from fruiting bodies in panel A. (C) The quantification of spore shape (spore length divided by the width) in untreated AX3 cells and AX3 cells treated with 600 μM BME (mean + SD). Student's *t* test was used to analyze significant changes in the shape of spores in BME-treated cells versus the AX3 control (untreated cells) (*, *P* value $\leq$ 0.05). This experiment was independently replicated 3 times. At least 100 spores from 4 fruiting bodies were measured each time.

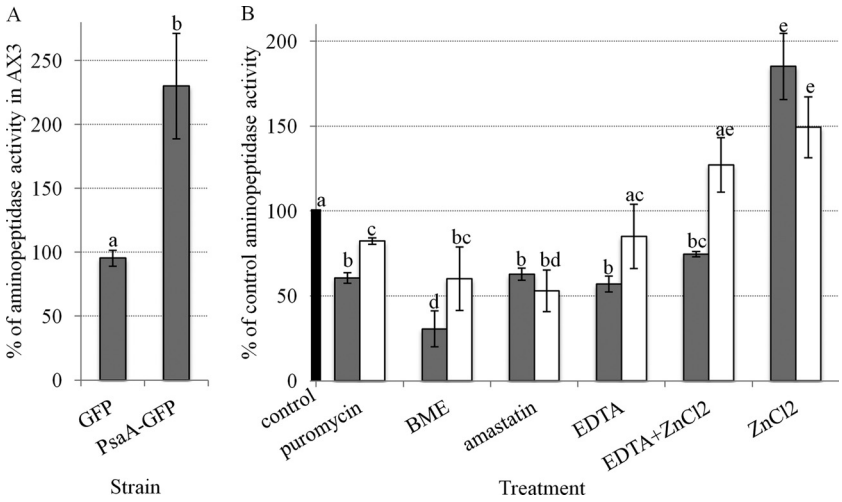

FIG 7 Aminopeptidase activity in PsaA-GFP-overexpressing cell lysates, and the effect of different agents on this activity. (A) Aminopeptidase activity in GFP and PsaA-GFP-overexpressing cell lysates measured as a percentage of activity in lysates of the parental AX3 cells (mean + SD). The aminopeptidase activity was measured fluorometrically by liberation of naphthylamide from alanine-β-naphthylamide by whole-cell lysates. Student's *t* test was used to analyze a significant change in aminopeptidase activity in PsaA-GFP- versus GFP-overexpressing cells (*, *P* value $\leq$ 0.05). (B) The effect of 200 μM puromycin, 300 μM BME, 20 μM amastatin, 5 mM EDTA, 5 mM EDTA + 10 μM $ZnCl_2$ and 10 μM $ZnCl_2$ on aminopeptidase activity in PsaA-GFP-overexpressing cell lysates (dark gray bars) and GFP-overexpressing cell lysates (white bars), expressed as a percentage of activity in these lysates with no added agent (black bar) (mean + SD). A one-way ANOVA with Tukey's test was used to analyze significant changes in aminopeptidase activity in PsaA-GFP- and GFP-overexpressing cell lysates compared to the untreated controls as well as in PsaA-GFP-overexpressing cell lysates compared to GFP alone. Data points that do not share a letter are statistically different (*P* value $\leq$ 0.05). This experiment was independently replicated 4 times, and each time the sample was measured twice.

after treatment with BME and EDTA. BME inhibited aminopeptidase activity in lysates of PsaA-GFP- and GFP-expressing cells by 69.39% $\pm$ 10.5% and 39.93% $\pm$ 18.7% of control, respectively. Aminopeptidase activity in PsaA-GFP-expressing cells was inhibited by EDTA by 43.00% $\pm$ 4.7% of control and in GFP-expressing cells by 14.90% $\pm$ 19.0% of control. On the other hand, aminopeptidase activity of both lysates was inhibited to the same degree by amastatin. It inhibited aminopeptidase activity in PsaA-GFP-expressing cells by 37.24% $\pm$ 3.6% and in GFP-expressing cells by 47.01% $\pm$ 12.2% of control. $ZnCl_2$ partially rescued the inhibition of aminopeptidase activity by EDTA in PsaA-GFP-expressing cells. Treatment of lysates of PsaA-GFP-expressing cells with EDTA and $ZnCl_2$ resulted in a 17.68% rescue in activity compared to treatment with EDTA alone. Both also rescued and even enhanced aminopeptidase activity in lysates of GFP-expressing cells by 27.24% $\pm$ 16.0% of untreated control. Treatment of lysates of PsaA-GFP- and GFP-expressing cells with $ZnCl_2$ alone enhanced aminopeptidase activity by 85.18% $\pm$ 19.4% and 49.35% $\pm$ 18.0% of control, respectively. Thus, lysates of PsaA-GFP-overexpressing cells are more sensitive to $ZnCl_2$ than lysates of GFP-overexpressing cells. This provides strong evidence that PsaA is a Zn^{2+}-binding puromycin-sensitive aminopeptidase the enzymatic activity of which is specifically inhibited by BME.

PsaA is differentially expressed throughout growth and development. Western and Northern blots were used to analyze expression levels of PsaA in growing and developing cells (Fig. 8A to D). PsaA protein levels were the highest in growing cells, decreased to 20 h of development and increased slightly by 24 h of development (Fig. 8A and C). Alpha-tubulin was used as a reference. PsaA mRNA levels followed a similar trend. PsaA mRNA levels decreased from levels found in growing cells to 16 h of development and increased again by 24 h of development (Fig. 8B and D). The mitochondrial large subunit rRNA, RnlA, was used as a developmental loading control, a standard in the field, and its levels did not change significantly throughout development.

PsaA expression is differentially regulated by developmental morphogens. AX3 cells were treated for up to 4 h with cAMP, NH_4Cl, DIF-1, or any two in combination (37). We have previously published the successful use of this method to assess developmental regulation of several proteins, including a known stalk cell marker acid phosphatase (37). Western blots of whole-cell extracts from treated and untreated cells were probed with anti-PsaA (Fig. 9A). Treatment of cells with cAMP for 4 h increased PsaA expression to 120.32% $\pm$ 9.7% of untreated control (Fig. 9B). Cotreatment of cells with cAMP and DIF-1 slightly inhibited this increase in expression. Treatment of cells with DIF-1 alone inhibited PsaA expression by approximately 20% (81.34% $\pm$ 6.5% of untreated control). Cotreatment of cells with cAMP and NH_4Cl inhibited PsaA expression to 82.94% $\pm$ 9.5% of untreated control. A similar level of inhibition was observed in cells treated with NH_4Cl alone. Cotreatment of cells with DIF-1 and NH_4Cl did not affect PsaA expression levels significantly. Thus, morphogens differentially regulate PsaA expression. PsaA expression was induced by cAMP but repressed by DIF-1 or NH_4Cl.

Overexpression of PsaA-GFP affects spore cell differentiation. The expression of PsaA-GFP, PsaAΔNLS2-GFP, or GFP did not affect growth or the timing of development (data not shown). Fruiting bodies formed by 24 h as by the parental AX3 strain. The fruiting bodies formed by each strain were stained with calcofluor for the examination of morphology of stalk and spore cells (Fig. 10A). Spore differentiation was significantly inhibited by the overexpression of PsaA-GFP but not PsaAΔNLS2-GFP or GFP alone since fruiting bodies formed by PsaA-GFP-expressing cells produced about 60% (38.4% $\pm$ 31.4% of cells in the spore masses were spores) fewer spores (Fig. 10B). Other cells appeared nonvacuolated and did not have a cellulose wall, thus they were likely

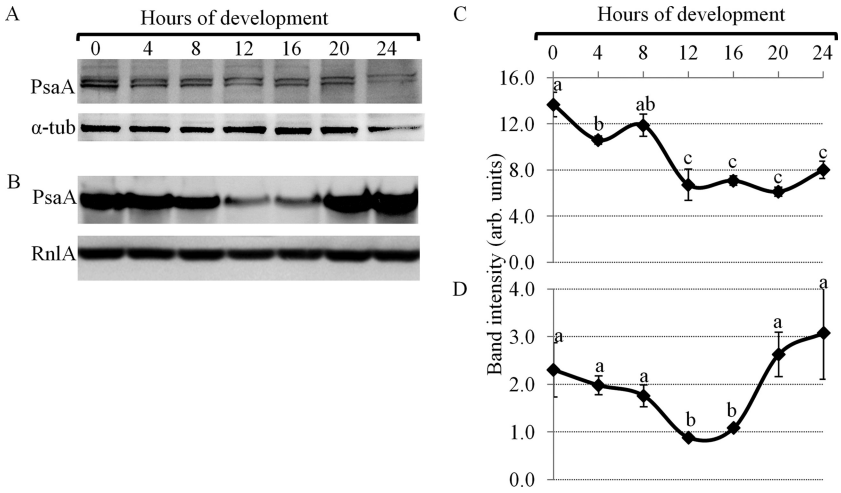

FIG 8 PsaA protein and mRNA expression during *D. discoideum* development. (A) A representative Western blot showing PsaA (98 kDa) protein levels in growing (0 h of development) and developing cells. (B) A representative Northern blot showing PsaA (2.58 kb) mRNA levels in growing and developing cells. RnlA (2.8 kb) mRNA levels were used as a loading control. (C and D) A quantification of band intensities of PsaA protein (C) and mRNA levels (D) from panels A and B, respectively (mean + SD). A one-way ANOVA with Tukey's test was used to analyze significant changes in protein and mRNA levels in developing cells. Data points that do not share a letter are significantly different (P value ≤ 0.05). This experiment was independently replicated 4 times.

prespore cells that did not undergo terminal differentiation into spores. In comparison, spores comprised 97.7% ± 1.2%, 97.8% ± 2.1%, and 99% ± 1.0% of cells in the spore masses of fruiting bodies formed by the parental AX3 cells and cells overexpressing PsaAΔNLS2-GFP or GFP, respectively. Stalk cell morphology (basal disc and stalk proper) was not affected by the overexpression (data not shown). PsaA-GFP-expressing spores that did terminally differentiate were rounder than spores formed by the parental AX3 cells (Fig. 10C). The shape was calculated by dividing the spore length by the width. Expression of PsaAΔNLS2-GFP or GFP did not affect spore shape. Thus, spore cell differentiation is affected by overexpression of PsaA-GFP in the nucleus but not the cytoplasm. The effect of PsaA-GFP overexpression resembles the effect of BME treatment in that both inhibit spore cell differentiation and result in rounded spores.

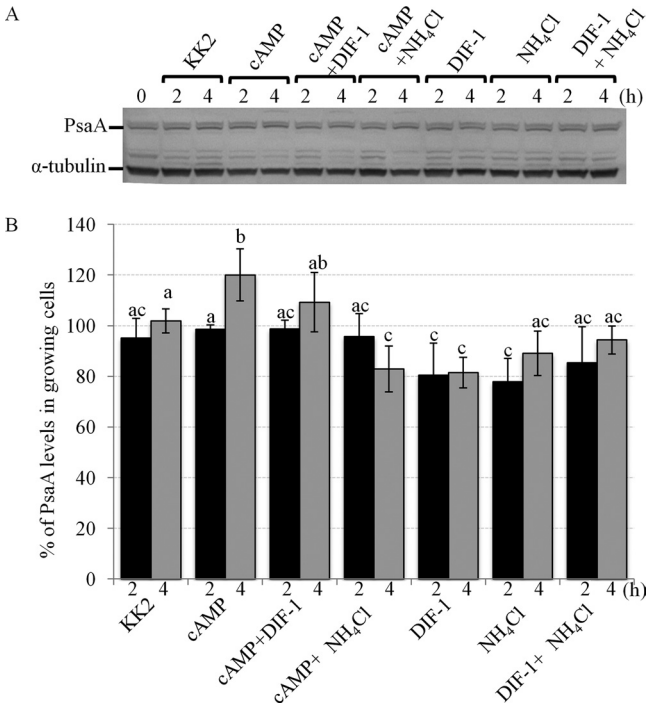

FIG 9 The effect of developmental morphogens on PsaA expression. Cells were starved (in KK_2) for 2 to 4 h in the presence or absence of cAMP, DIF-1, NH_4Cl, or any two in combination. (A) Western blot showing PsaA and α-tubulin expression in treated cells. (B) The quantification of band intensities from Western blot in panel A (mean + SD). A two-way ANOVA with Tukey's test was used to analyze changes in band intensities. Different treatments were compared at each time point, and different time points were compared within each treatment. Groups that do not share a letter are statistically different (P value ≤ 0.05). This experiment was independently replicated 4 times.

Cells overexpressing PsaA-GFP or PsaAΔNLS2-GFP have a sorting defect. To further analyze the effect of PsaA overexpression, chimeras were generated. PsaA-GFP-expressing cells were mixed in a range of ratios with parental AX3 cells (1:9 to 9:1). The sorting defect was most clearly visible when a ratio of GFP-expressing cells to parental AX3 cells was 2:8. Development was followed for 24 h to see if overexpressing cells show sorting defects and thus differentiation defects. In chimeric slugs (16 h of development), PsaA-GFP-expressing cells sorted to both the anterior of slugs, specifically the posterior of prestalk zone, and to the posterior of slugs, the posterior portion of prespore zone (Fig. 11A and B). PsaAΔNLS2-GFP-expressing cells localized primarily to the prespore zone (Fig. 11A and B). GFP-expressing cells did not sort preferentially into a specific zone of the slug but rather were dispersed throughout the whole slug (Fig. 11A and B). These sorting patterns were quantified by analyzing fluorescence levels along the length of slugs (all slugs standardized to the length of 1) using the NIS profile tool, a technique that could be of tremendous benefit to the field.

PsaA-GFP- and PsaAΔNLS2-GFP-overexpressing cells preferentially differentiate into stalk or spore cells, respectively. The sorting defects of PsaA-overexpressing cells in chimeras were further analyzed at 24 h of development in fruiting bodies. PsaA-GFP-expressing cells were found mainly in the lower and upper cup, the stalk and the basal disc, but not the spore mass of chimeric fruiting bodies (Fig. 12A and B). PsaAΔNLS2-GFP-expressing

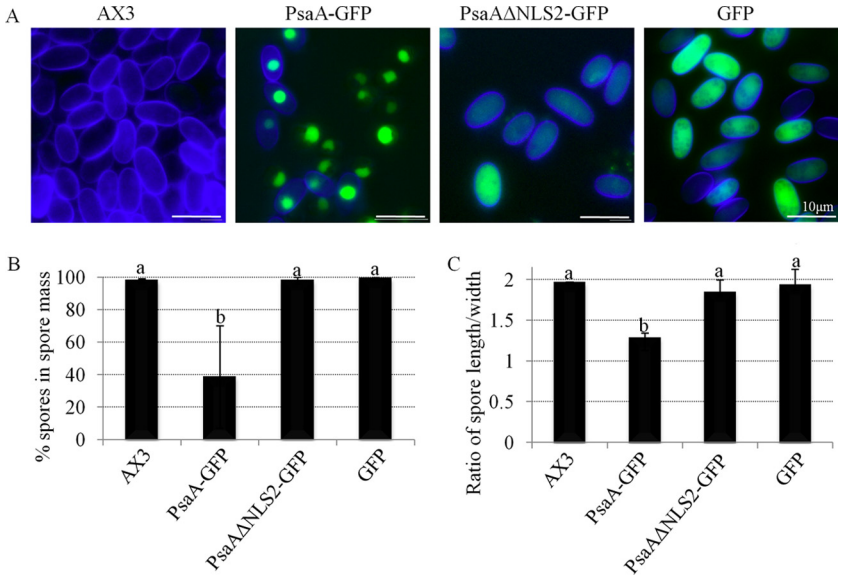

FIG 10 The effect of overexpression of PsaA on spore cell differentiation in *D. discoideum*. (A) Morphology of calcofluor-stained spore mass cells overexpressing PsaA-GFP, PsaAΔNLS2-GFP, GFP alone, or nothing (parental AX3). Blue, calcofluor-stained spore coats; green, GFP. (B) Percent of cells in the spore masses of fruiting bodies formed by the above strains that appear as spores (stained with calcofluor and are not vacuolized; mean + SD). (C) The ratio of the length over the diameter of spores formed by the above strains (mean + SD). A one-way ANOVA with Tukey's test was used to analyze significant changes in the number of spores formed (A) and their shape (B) in overexpressing strains versus the parental AX3 (raw values were used for the statistical analysis). Data points that do not share a letter are statistically different (P value ≤ 0.05). At least 100 spores from 3 fruiting bodies (of each strain) were counted and measured. This experiment was independently replicated 4 times.

cells were mainly found in the spore mass. In contrast, GFP-expressing cells were found throughout the fruiting body, in the basal disc, stalk, spore mass, and cup areas. Spore differentiation was quantified in the chimeras. The expected percentage of fluorescent spores, if the cells did not show a differentiation preference, is 20%. GFP-expressing cells made up 21.1% ± 3.4% of the spores in chimera fruiting bodies (Fig. 12C). PsaA-GFP-overexpressing cells only comprised 0.3% ± 0.6% of spores in the spore mass, while PsaAΔNLS2-GFP made up 43.95% ± 5.5% of the spores. Thus, nuclear versus cytoplasmic overexpression of PsaA resulted in a bias in the differentiation pathway.

The effect of BME treatment on cells overexpressing PsaA-GFP. GFP fusion protein-overexpressing cells were allowed to develop on filters soaked in 600 or 900 μM BME. Cells expressing PsaAΔNLS2-GFP developed normally and formed fruiting bodies by 24 h (Fig. 13A). Spores formed by PsaAΔNLS2-GFP-expressing

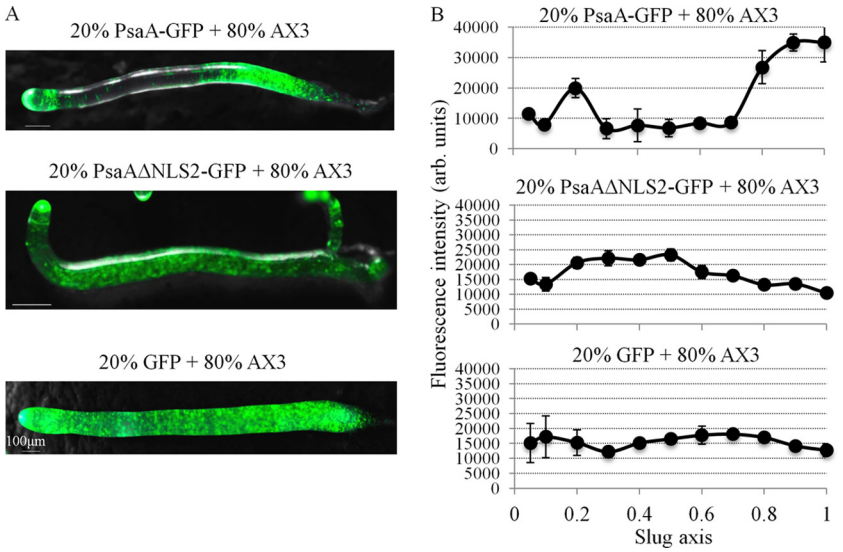

FIG 11 The effect of overexpression of PsaA on cell sorting in *D. discoideum*. (A) Slugs composed of 20% of cells overexpressing PsaA-GFP, PsaAΔNLS2-GFP, or GFP alone and 80% of parental AX3 cells. Phase images with GFP fluorescence overlay are shown. Slug tips are to the left. (B) Quantification of fluorescence over the slug's length in panel A (mean + SD). The tip corresponds to zero on the slug axis. Fluorescence was quantified in 5 slugs from 3 independent experiments.

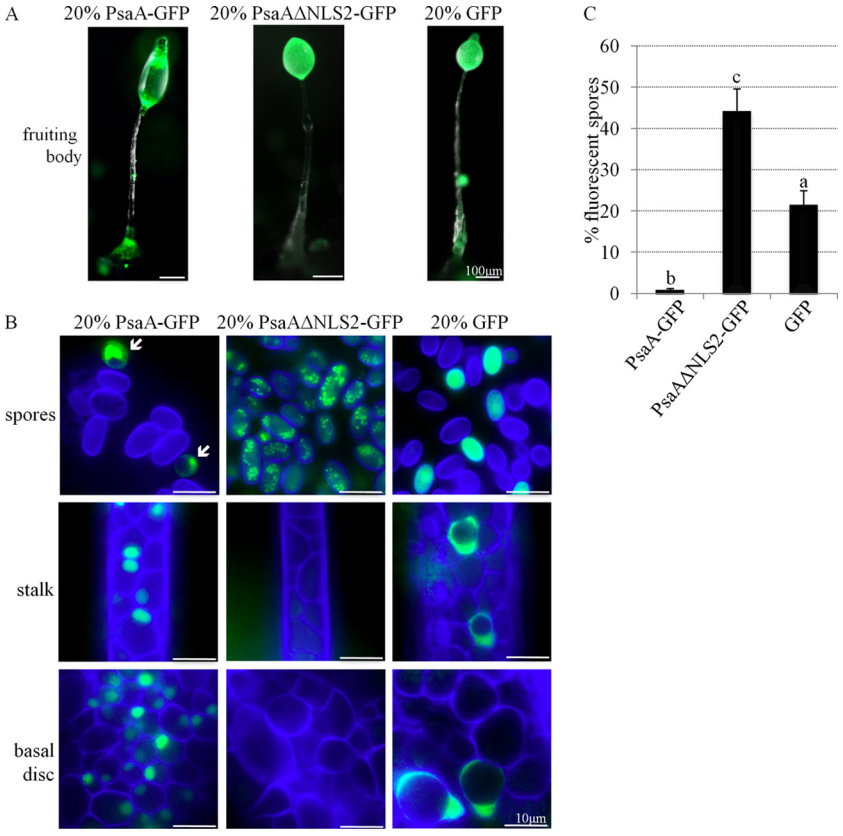

FIG 12 The effect of overexpression of PsaA on cell sorting in *D. discoideum* as observed in fruiting bodies. (A) Fruiting bodies composed of 20% of cells overexpressing PsaA-GFP, PsaAΔNLS2-GFP, or GFP alone and 80% of parental AX3 cells. Phase images with GFP fluorescence overlay are shown. (B) Calcofluor-stained spores (blue), stalk, and basal disc cells of fruiting bodies in panel A. Arrows in the first panel point to small, partially vacuolated, fluorescent cells that are likely cup cells. (C) Quantification of the number of fluorescent spore in panel B as a percentage of total number of spores (mean + SD). A one-way ANOVA with Tukey's test was used to analyze significant changes in the number of fluorescent spores. Data points that do not share a letter are statistically different (P value ≤ 0.05). At least 10 fruiting bodies from 3 independent replicates were viewed. At least 100 spores/fruiting bodies were counted.

cells treated with 600 μM BME were rounded in shape compared to untreated control (Fig. 13B and C). BME at 900 μM inhibited terminal spore cell differentiation, as very few (and round) spores were formed by treated PsaAΔNLS2-GFP-expressing cells (Fig. 13B). The same effect of BME was observed on cells overexpressing GFP alone (data not shown).

The effect of BME on PsaA-GFP-expressing cells was more severe than the effect of overexpression alone or the effect of BME

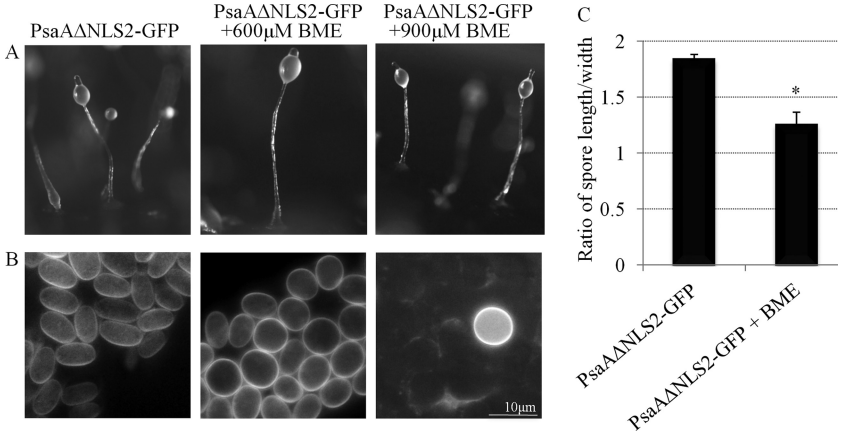

FIG 13 The effect of BME on development of PsaAΔNLS2-GFP-overexpressing cells. (A) Fruiting bodies formed by 24 h by untreated PsaAΔNLS2-GFP-expressing cells and these cells treated with 600 or 900 μM BME. (B) Calcofluor-stained spores from fruiting bodies in panel A. (C) The quantification of spore shape (the spore length divided by the width) in untreated PsaAΔNLS2-GFP-expressing cells or cells treated with 600 μM BME (mean + SD). Student's t test was used to analyze significant changes in the shape of spores in BME-treated cells versus untreated cells (*, P value ≤ 0.05). This experiment was independently replicated 3 times. At least 100 spores from 4 fruiting bodies were measured each time.

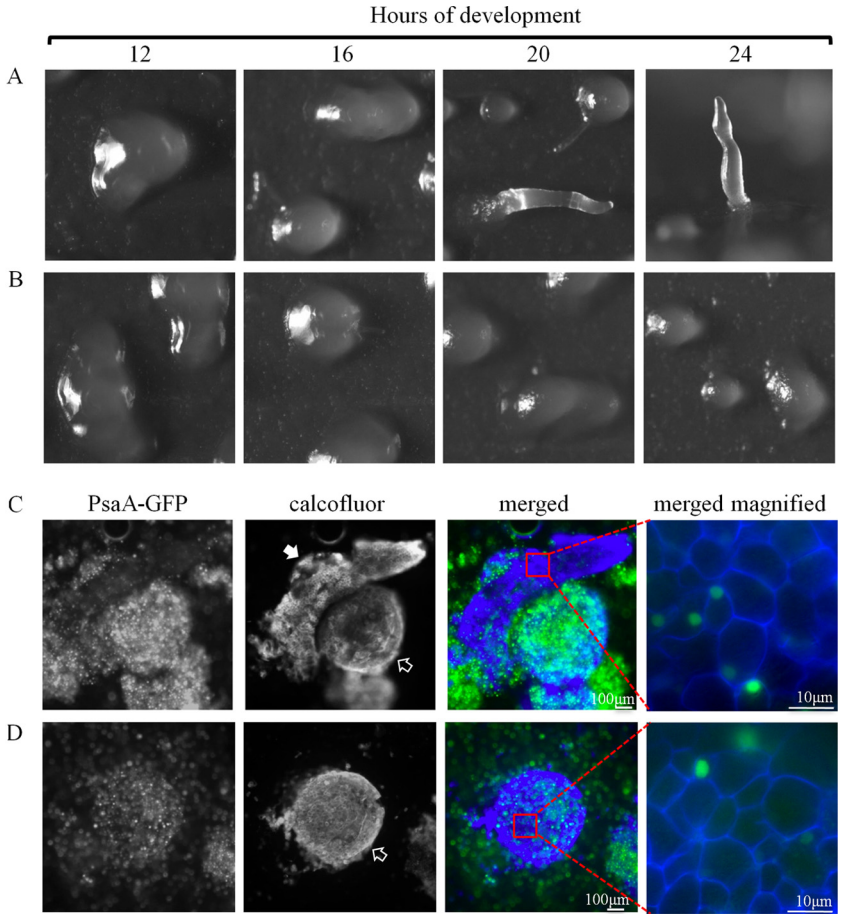

FIG 14 The effect of BME on development of PsaA-GFP-overexpressing cells. A developmental sequence of PsaA-GFP-expressing cells treated with 600 (A) or 900 (B) μM BME and allowed to develop on filters for up to 24 h. The 24-h image in panel A is a side view; the rest of the images are top views. (C and D) Calcofluor-stained cells of the structures formed on 600 (C) and 900 (D) μM BME at 24 h. These correspond to structures seen at 24 h in panels A and B, respectively. Solid arrow points to finger, and empty arrows point to mounds. The last images in panels C and D show the stalk cells that comprise these structures. This experiment was independently replicated 4 times. At least 10 finger- and mound-like structures were stained and viewed each time.

on PsaAΔNLS2-GFP-expressing cells or the parental AX3. Cells expressing PsaA-GFP treated with 600 and 900 μM BME developed abnormally, and no fruiting bodies were formed by 24 h (Fig. 14A, B). At both concentrations of BME, cells aggregated to form large- and irregular-shaped mounds that often broke apart later on in the development. At 600 μM BME, some of the mounds extended to form fingers (Fig. 14A). Some of the fingers fell over and resembled slugs but did not migrate on the filters. By 24 h, some standing fingers were observed. After staining with calcofluor, it was evident that all cells of the mounds and fingers were terminally differentiated stalk cells (Fig. 14C). Similarly, at 900 μM BME, development was completely arrested at the mound stage (Fig. 14B) and all cells of the mounds were comprised of terminally differentiated stalk cells (Fig. 14D). No spores were observed at 600 or 900 μM BME.

DISCUSSION

Here we have gained insight into the effect of BME treatment and the role of PsaA, a NumA1, and Cdk5 binding partner in growth and development of *D. discoideum*. The treatment of cells with BME decreased the rate of cell growth and the frequency of cell division and inhibited normal spore cell differentiation. Overexpression of PsaA-GFP also disrupted normal spore cell differentiation. We showed that BME likely binds to and specifically inhibits the enzymatic activity of PsaA. Additionally, nuclear and cytoplasmic PsaA may play different roles in stalk and spore cell differentiation. In chimeras, when cells overexpressed PsaA-GFP they differentiated into stalk cells, but when they overexpressed PsaAΔNLS2-GFP they differentiated into spores. Interestingly, the developmental effect of BME was more severe in PsaA-GFP-expressing cells than in the parental AX3, where development was arrested and cells differentiated only into stalk cells and no spores were ever formed.

Evidence that BME specifically interacts with and inhibits PsaA enzymatic activity. Anti-PsaA was unable to detect PsaA when cells were treated with BME, but the fluorescence from PsaA-GFP was still visible. This suggests that BME does not decrease the amount of nuclear PsaA but rather interacts directly with PsaA, blocking antibody binding. BME also inhibited aminopeptidase activity more in PsaA-GFP-expressing cells than GFP-expressing cells, again suggesting an interaction between BME and PsaA, as well as specific inhibition of PsaA's enzymatic activity by BME. Further work is needed to show that BME is a specific inhibitor of PsaA in *D. discoideum*, but it is likely that the

effects of BME on growth and differentiation were the result of PsaA inhibition. *D. discoideum* cells also possess a closely related PsaB gene. While no research has been done on PsaB, it is possible that it did not contribute to the results of this study. First, the antibody used here is specific for PsaA and does not detect PsaB (7). Second, most significant results relate to the PsaA-GFP- and PsaAΔNLS2-GFP-overexpressing strains and not to the endogenous PsaA, or potential endogenous PsaB, activity in the parental strain.

Evidence that PsaA has a role in cell cycle regulation. Since the treatment of cells with BME resulted in the slower progression through the cell cycle due to decreased rate of cell growth and the frequency of cell division, PsaA likely has a role in cell cycle regulation. This fits with the proposed cell cycle role of PSA in mammalian cells and the known interaction of PsaA with NumA1 and Cdk5 in *D. discoideum* (7, 10, 17). Bestatin has also been shown to inhibit proliferation of COS cells, Swiss 3T3 fibroblasts, and primary hepatocytes (10, 47, 48). As mentioned previously, bestatin is also used as an antitumor agent for its antiproliferative, proapoptotic, and antiangiogenic properties.

PsaA and spore cell differentiation. The inhibition of spore differentiation in BME-treated cells and cells expressing PsaA-GFP reveals that PsaA also has a role in spore cell differentiation. The PsaA RNA and protein expression profiles are in agreement with a role for PsaA in growing cells and during late development, when spore cells are undergoing terminal differentiation, as the levels of PsaA are the highest at those points. Several developmentally regulated aminopeptidases have been shown to exist in *D. discoideum* (8, 13, 36). However, PsaA is the first whose function has been characterized to any extent (7). Further support for the role of PsaA in spore cell differentiation comes from the fact that PsaA expression was specifically induced by cAMP but repressed by DIF-1 and ammonia. During development cAMP regulates spore cell differentiation while DIF-1 regulates stalk cell differentiation (54).

PsaA is a puromycin-sensitive aminopeptidase. The aminopeptidase assay demonstrated that this enzyme is a true puromycin-sensitive aminopeptidase with attributes common to this enzyme as seen in other organisms. It is an alanyl-aminopeptidase that is sensitive to puromycin, BME, amastatin, and EDTA, all attributes of puromycin-sensitive aminopeptidase. Similarly, it requires $ZnCl_2$ for its activity. PsaA-GFP-expressing cells have more aminopeptidase activity than cells expressing GFP alone, and this activity is more sensitive to puromycin, BME, EDTA, and $ZnCl_2$ but not amastatin. Like bestatin, amastatin is a metallopeptidase inhibitor but it has different specificity toward aminopeptidases than bestatin. For example, aminopeptidase A is very sensitive to amastatin but not bestatin. Amastatin and bestatin also elicit different cellular responses in different cell types (19, 45). Overexpression of PsaA in the PsaA-GFP strain has been verified by Western blotting, demonstrating approximately a 4-fold overexpression of fusion proteins in comparison to native PsaA (7). This provides strong evidence that both endogenous and expressed PsaA are functional Zn^{2+}-binding puromycin-sensitive aminopeptidases that can cleave alanine. In keeping with this, BME specifically inhibits both endogenous and expressed PsaA activity. PSA in COS cells and human liver cytosol has previously been shown to cleave alanine from substrates (10, 56). Additionally, alanine specific aminopeptidase had previously been detected in developing *D. discoideum* cells but remained uncharacterized (36).

Overexpression of PsaA-GFP and treatment with BME have the same developmental effect. Overexpression of PsaA-GFP had the same effect on spore cell differentiation as the treatment of cells with BME. The effect of BME was also more severe in the PsaA-GFP strain than the parental AX3 such that morphogenesis was inhibited and cells differentiated only into stalk cells with no spore differentiation. Inhibition is usually rescued by overexpression but not in this case. Immunolocalization and aminopeptidase assay both suggest that BME specifically inhibits PsaA. It is possible that BME inhibits PsaA in a specific conformation. For example, BME may inhibit cytoplasmic but not nuclear PsaA. BME may also inhibit PsaB, but as alluded to above, the role of PsaB in *D. discoideum* development is not known. Additionally, any agents that affect PsaA activity may affect proper spore cell differentiation, suggesting that PsaA levels are tightly regulated during development. Alternatively, although the aminopeptidase assay suggests that PsaA is enzymatically active, it is still possible that PsaA-GFP acts as a dominant negative agent, antagonizing native PsaA function. If this is true, then nuclear PsaA is essential for proper spore cell differentiation. Future analysis of the developmental phenotype of PsaA knockout cells will clarify this issue.

Overexpression of PsaA causes a sorting defect. Differential sorting of cells expressing PsaA-GFP or PsaAΔNLS2-GFP also suggests that nuclear and cytoplasmic PsaA play different roles in cell differentiation. Overexpression of PsaA-GFP inhibits spore cell differentiation. Fittingly, in chimeras, PsaA-GFP-expressing cells do not sort to the prespore zone and do not differentiate into spores. Others have shown that mutants with compromised ability to form functional spores also do not sort to the prespore zone or differentiate into spores in chimeras with parental cells (35). On the other hand, cells that overexpress PsaAΔNLS2-GFP, preferentially sort to the prespore zone and differentiate into spores.

It is of interest to note that 43.95% ± 5.5% of spores expressed PsaAΔNLS2-GFP when only 20% of these cells were mixed with 80% parental AX3 cells. About 80% of cells in each aggregate are expected to differentiate into spores, so if all PsaAΔNLS2-GFP-expressing cells differentiated into spores, then they should have comprised 25% of spores in the spore mass. This phenomenon could be explained by the observation that slugs containing PsaAΔNLS2-GFP-expressing cells were significantly smaller than control slugs (data not shown). One explanation is that PsaAΔNLS2-GFP expression has a nonautonomous effect on cells, altering cell aggregation abilities. This remains to be elucidated in detail in future studies. Thus, overexpression of nuclear PsaA (PsaA-GFP) drives cells to the stalk cell pathway while overexpression of cytoplasmic PsaA (PsaAΔNLS2-GFP) drives cells to the spore cell pathway. Cell fractionation into nuclear and cytoplasmic fragments and analysis of PsaA in both will help elucidate the relationship between nuclear and cytoplasmic PsaA in cell differentiation. It is not clear why the overexpression of PsaA-GFP or PsaAΔNLS2-GFP did not have an effect on cell culture growth. Evidently, further work is needed to clarify the role of PsaA in growth and development but it is clear that PsaA is likely important in both events.

PsaA may be functionally linked to Cdk5. Further support for the role of PsaA in cell differentiation comes from the observation that effects of Cdk5 inhibition strongly resemble the effects of PsaA overexpression or the treatment of cells with BME. PsaA is a

binding partner of Cdk5 (17). *D. discoideum* cells expressing a dominant negative form of Cdk5 grow 3 times slower and produce 80% less spores than the wild type (46). Treatment of cells with roscovitine, an inhibitor of Cdks, also inhibits *D. discoideum* growth and spore cell differentiation (18). Overexpression of Cdk5 rescues normal growth in roscovitine-treated cells. This suggests that PsaA and Cdk5 are functionally linked both during growth and development. Both likely regulate cell cycle events and spore cell differentiation. Further analysis of PsaA's role in growth and development will help elucidate this link.

In conclusion, *D. discoideum* provides a simple model system for the analysis of effects of BME on cell growth, division, and differentiation and the role of PsaA in these processes. Further analysis of PsaA function and effect of BME treatment in *D. discoideum* will provide invaluable insight into these processes and the mode of action of BME in normal and diseased cells.

ACKNOWLEDGMENTS

This work was supported by the Natural Sciences and Engineering Research Council of Canada (D.H.O.; grant no. A6807).

REFERENCES

1. **Alba F, Iríbar C, Ramírez M, Arenas C.** 1989. A fluorimetric method for the determination of brain aminopeptidases. Arch. Neurobiol. (Madr.) **52**:169–173.
2. **Aozuka Y, et al.** 2004. Anti-tumor angiogenesis effect of aminopeptidase inhibitor bestatin against B16-BL6 melanoma cells orthotopically implanted into syngeneic mice. Cancer Lett. **216**:35–42.
3. **Bhutani N, Venkatraman P, Goldberg AL.** 2007. Puromycin-sensitive aminopeptidase is the major peptidase responsible for digesting polyglutamine sequences released by proteasomes during protein degradation. EMBO J. **26**:1385–1396.
4. **Brooks DR, Hooper NM, Isaac RE.** 2003. The *Caenorhabditis elegans* orthologue of mammalian puromycin-sensitive aminopeptidase has roles in embryogenesis and reproduction. J. Biol. Chem. **278**:42795–42801.
5. **Burley SK, David PR, Lipscomb WN.** 1991. Leucine aminopeptidase: Bestatin inhibition and a model for enzyme-catalyzed peptide hydrolysis. Proc. Natl. Acad. Sci. U. S. A. **88**:6916–6920.
6. **Catalano A, O'Day DH.** 2011. Nucleolar localization and identification of nuclear/nucleolar localization signals of the calmodulin-binding protein nucleomorphin during growth and mitosis in *Dictyostelium.* Histochem. Cell Biol. **135**:239–249.
7. **Catalano A, Poloz Y, O'Day DH.** 2011. *Dictyostelium* puromycin-sensitive aminopeptidase A is a nucleoplasmic nucleomorphin-binding protein that relocates to the cytoplasm during mitosis. Histochem. Cell Biol. **136**:677–688.
8. **Chan SA, Toursarkissian K, Sweeney JP, Jones TH.** 1985. Dipeptidyl-aminopeptidases and aminopeptidases in *Dictyostelium discoideum.* Biochem. Biophys. Res. Commun. **127**:962–968.
9. **Chen X, et al.** 2003. Leukotriene A4 hydrolase in rat and human esophageal adenocarcinomas and inhibitory effects of bestatin. J. Natl. Cancer Inst. **95**:1053–1061.
10. **Constam DB, et al.** 1995. Puromycin-sensitive aminopeptidase. Sequence analysis, expression, and functional characterization. J. Biol. Chem. **270**:26931–26939.
11. **Ezawa K, Minato K, Dobashi K.** 1996. Induction of apoptosis by ubenimex (Bestatin) in human non-small-cell lung cancer cell lines. Biomed. Pharmacother. **50**:283–289.
12. **Fey P, Kowal AS, Gaudet P, Pilcher KE, Chisholm RL.** 2007. Protocols for growth and development of *Dictyostelium discoideum.* Nat. Protoc. **2**:1307–1316.
13. **Firtel RA, Brackenbury RW.** 1972. Partial characterization of several protein and amino acid metabolizing enzymes in the cellular slime mold *Dictyostelium discoideum.* Dev. Biol. **27**:307–321.
14. **Firtel RA, Meili R.** 2000. *Dictyostelium*: a model for regulated cell movement during morphogenesis. Curr. Opin. Genet. Dev. **10**:421–427.
15. **Fujisaki T, et al.** 2003. Bestatin selectively suppresses the growth of leukemic stem/progenitor cells with BCR/ABL mRNA transcript in patients with chronic myelogenous leukemia. Int. Immunopharmacol. **3**:901–907.
16. **Harrington BJ, Raper KB.** 1968. Use of a fluorescent brightener to demonstrate cellulose in the cellular slime molds. Appl. Microbiol. **16**:106–113.
17. **Huber RJ, O'Day DH.** 2011. Nucleocytoplasmic transfer of cyclin dependent kinase 5 and its binding partner puromycin-sensitive aminopeptidase in *Dictyostelium discoideum.* Histochem. Cell Biol. **136**:177–189.
18. **Huber RJ, O'Day DH.** 2011. The cyclin-dependent kinase inhibitor roscovitine inhibits kinase activity, cell proliferation, multicellular development, and Cdk5 nuclear translocation in *Dictyostelium discoideum.* J. Cell. Biochem. **113**:868–876.
19. **Hui K, Saito M, Hui M.** 1998. A novel neuron-specific aminopeptidase in rat brain synaptosomes. Its identification, purification, and characterization. J. Biol. Chem. **273**:31053–31060.
20. **Ichinose Y, et al.** 2003. Randomized double-blind placebo-controlled trial of bestatin in patients with resected state I squamous-cell lung carcinoma. J. Natl. Cancer Inst. **95**:605–610.
21. **Inoi K, et al.** 1995. Aminopeptidase inhibitor ubenimex (bestatin) inhibits the growth of human choriocarcinoma in nude mice through its direct cytostatic activity. Anticancer Res. **15**:2081–2087.
22. **Koonce MP.** 2000. *Dictyostelium*, a model organism for microtubule-based transport. Protist **151**:17–25.
23. **Koonce MP, Gräf R.** 2010. *Dictyostelium discoideum.* A model system for ultrastructural analyses of cell motility and development. Methods Cell Biol. **96**:197–216.
24. **Kudo LC, et al.** 2011. Puromycin-sensitive aminopeptidase (PSA/NPEPPS) impedes development of neuropathology in HPSA/TAUP301L double-transgenic mice. Hum. Mol. Genet. **20**:1820–1833.
25. **Lin M, He J, Cai Z, Qian W.** 2001. Aminopeptidase inhibitor Bestatin induces HL-60 cell apoptosis through activating caspase 3. Zhonghua Xue Ye Xue Za Zhi. **22**:348–350.
26. **Lkhagvaa B, et al.** 2008. Bestatin, an inhibitor for aminopeptidases, modulates the production of cytokines and chemokines by activated monocytes and macrophages. Cytokine **44**:386–391.
27. **Lyczak R, et al.** 2006. The puromycin-sensitive aminopeptidase PAM-1 is required for meiotic exit and anteroposterior polarity in the one-cell *Caenorhabditis elegans* embryo. Development (Camb.) **133**:4281–4292.
28. **Matsumoto T, et al.** 1991. Relationship between nucleolar size and growth characteristics in small cell lung cancer cell lines. Japan. J. Cancer Res. **82**:820–828.
29. **McMains VC, Myre M, Kreppel L, Kimmel AR.** 2010. *Dictyostelium* possesses highly diverged presenilin/γ-secretase that regulates growth and cell-fate specification and can accurately process human APP: a system for functional studies of the presenilin/γ-secretase complex. DNM Dis. Models Mech. **3**:581–594.
30. **Murata Y, et al.** 2003. Bestatin results in pathophysiological changes similar to preeclampsia in rats via induction of placental apoptosis. Horm. Metab. Res. **35**:343–348.
31. **Myre MA, et al.** 2011. Deficiency of huntingtin has pleiotropic effects in the social amoeba *Dictyostelium discoideum.* PLoS Genet. **7**:e1002052.
32. **Myre MA, O'Day DH.** 2002. Nucleomorphin. A novel, acidic, nuclear calmodulin-binding protein from *Dictyostelium* that regulates nuclear number. J. Biol. Chem. **277**:19735–19744.
33. **Myre MA, O'Day DH.** 2004. *Dictyostelium* nucleomorphin is a member of the BRCT-domain family of cell cycle checkpoint proteins. Biochim. Biophys. Acta Gen. Subj. **1675**:192–197.
34. **Myre MA, O'Day DH.** 2004. *Dictyostelium* calcium-binding protein 4a interacts with nucleomorphin, a BRCT-domain protein that regulates nuclear number. Biochem. Biophys. Res. Commun. **322**:665–671.
35. **Niswonger ML, O'Halloran TJ.** 1997. Clathrin heavy chain is required for spore cell but not stalk cell differentiation in *Dictyostelium discoideum.* Development **124**:443–451.
36. **North MJ.** 1982. Proteolytic activities in *Dictyostelium discoideum* detected with chromogenic peptide substrates. Exp. Mycol. **6**:345–352.
37. **O'Day DH, Poloz Y, Myre MA.** 2009. Differentiation inducing factor-1 (DIF-1) induces gene and protein expression of the *Dictyostelium* nuclear calmodulin-binding protein nucleomorphin. Cell. Signal. **21**:317–323.
38. **Osada T, et al.** 2001. Male reproductive defects caused by puromycin-sensitive aminopeptidase deficiency in mice. Mol. Endocrinol. **15**:960–971.
39. **Osada T, Watanabe G, Sakaki Y, Takeuchi T.** 2001. Puromycin-sensitive aminopeptidase is essential for the maternal recognition of pregnancy in mice. Mol. Endocrinol. **15**:882–893.

40. **Peer WA.** 2011. The role of multifunctional M1 metallopeptidases in cell cycle progression. Ann. Bot. **107**:1171–1181.
41. **Poloz Y, O'Day DH.** 2012. Colchicine affects cell motility, pattern formation and stalk cell differentiation in *Dictyostelium* by altering calcium signaling. Differentiation **83**:185–199.
42. **Rawlings ND, Barrett AJ.** 1995. Evolutionary families of metallopeptidases. Methods Enzymol. **248**:183–228.
43. **Sánchez-Morán E, Jones GH, Franklin FCH, Santos JL.** 2004. A puromycin-sensitive aminopeptidase is essential for meiosis in *Arabidopsis thaliana*. Plant Cell **16**:2895–2909.
44. **Schulz C, Perezgasga L, Fuller MT.** 2001. Genetic analysis of dPsa, the *Drosophila* orthologue of puromycin-sensitive aminopeptidase, suggests redundancy of aminopeptidases. Dev. Genes Evol. **211**:581–588.
45. **Sekine K, Fujii H, Abe F.** 1999. Induction of apoptosis by bestatin (ubenimex) in human leukemic cell lines. Leukemia **13**:729–734.
46. **Sharma SK, et al.** 2002. The Cdk5 homologue, Crp, regulates endocytosis and secretion in *Dictyostelium* and is necessary for optimum growth and differentiation. Dev. Biol. **247**:1–10.
47. **Takahashi S, Kato H, Seki T.** 1985. Bestatin, a microbial aminopeptidase inhibitor, inhibits DNA synthesis induced by insulin or epidermal growth factor in primary cultured rat hepatocytes. J. Antibiot. **38**:1767–1773.
48. **Takahashi S, et al.** 1989. The effects of bestatin, a microbial aminopeptidase inhibitor, on epidermal growth factor-induced DNA synthesis and cell division in primary cultured hepatocytes of rats. Exp. Cell Res. **183**: 399–412.
49. **Taylor A.** 1993. Aminopeptidases: structure and function. FASEB J. **7**:290–298.
50. **Terbach N, et al.** 2011. Identifying an uptake mechanism for the antiepileptic and bipolar disorder treatment valproic acid using the simple biomedical model *Dictyostelium*. J. Cell Sci. **124**:2267–2276.
51. **Ueda M, Ueki M, Fujii H, Yoshizawa K, Nakajima M.** 1997. Inhibitory effects of ubenimex (bestatin) on the invasion of uterine cervical carcinoma cells and their production and activation of gelatinase A. J. Med. **28**:175–190.
52. **Umezawa H, Aoyagi T, Suda H, Hamada M, Takeuchi T.** 1976. Bestatin, an inhibitor of aminopeptidase B, produced by actinomycetes. J. Antibiot. **29**:97–99.
53. **Williams JG.** 2010. *Dictyostelium* finds new roles to model. Genetics **185**: 717–726.
54. **Williams JG.** 2006. Transcriptional regulation of *Dictyostelium* pattern formation. EMBO J. **7**:694–698.
55. **Yamada S, et al.** 2003. Effect of bestatin on leukemic cells in acute leukemia and myelodysplastic syndromes. Biotherapy (Japan) **17**:161–166.
56. **Yamamoto M, et al.** 2002. Axonal transport of puromycin-sensitive aminopeptidase in rat sciatic nerves. Neurosci. Res. **42**:133–140.